INSTITUTE OF PHYSICS PUBLISHING JOURNAL OF MICROMECHANICS AND MICROENGINEERING

J. Micromech. Microeng. **14** (2004) 138–146 PII: S0960-1317(04)64721-8

# Moving reflector type micro optical switch for high-power transfer in a MEMS-based safety and arming system

**Kevin R Cochran**[1,2], **Lawrence Fan**[2] **and Don L DeVoe**[1]

[1] Department of Mechanical Engineering, University of Maryland College Park, MD 20742, USA
[2] Indian Head Division, Naval Surface Warfare Center, Bldg 302, 101 Strauss Avenue, Indian Head, MD 20640, USA

E-mail: cochrankr@ih.navy.mil

Received 12 June 2003, in final form 18 September 2003
Published 14 October 2003
Online at stacks.iop.org/JMM/14/138 (DOI: 10.1088/0960-1317/14/1/019)

**Abstract**
Development of a moving reflector type micro optical switch fabricated by deep reactive ion etching (DRIE) in silicon on insulator (SOI) substrates is presented. The device discussed is a key component in a MEMS-based safety and arming (S&A) system for use in underwater weapons. In this switch, an etched vertical sidewall reflector is electrostatically actuated in and out of the optical path between input and output optical fibers. Fabrication is performed on 100 $\mu$m thick silicon substrates with fiber alignment channels, reflectors and actuators being fabricated at the same time with a single etch step. A single pair of multimode fibers is used to transmit optical power of the order of 1000 mW at a working wavelength of 810 nm. Sources of optical loss in the system are identified and their value calculated in order to predict the overall system optical efficiency. The optical efficiency of the switch has been found to have an average value of 55% with the etched vertical sidewall mirror having an average reflectivity of 62.8%. Switching time is 10 ms from the off to the on state with a maximum operational frequency of 60 Hz. Isolation between the on and off states is 32 dB.

## 1. Introduction

An optical micro switch for high-power transfer has been developed for integration into a MEMS-based safety and arming (S&A) system. The S&A system is currently being developed by the Indian Head Division, Naval Surface Warfare Center and is intended for use in underwater weapons. The purpose of the S&A system is to prevent unintended detonation of a weapon while ensuring that detonation will reliably take place when needed. The first generation of the MEMS S&A device used LIGA processing to create a movable barrier that physically interrupted an explosive train initiator [1].

This paper describes the second-generation device in which the electrical power to the initiator system is interrupted by optical means. The system provides fail-safe activation and termination of an optical path between a low-power source and a high-power discharge capacitor. A schematic of the system is shown in figure 1.

A key component to this system is a MEMS-based optical interrupter chip. The interrupter has been investigated previously using LIGA processing [2]. The optical output from a laser diode (LD) is fed to the interrupter chip through an input optical fiber. On-chip components include an optical switch along with environmental sensors and locks, which are necessary for proper S&A system operation. The optical output from the interrupter is sent to a photodetector through an output optical fiber. The electrical output from the photodetector is in turn sent to a power conversion circuit and finally to a high-voltage discharge capacitor.

In order for the discharge capacitor to charge sufficiently, the output photodetector must provide 5 V and 80–100 mA for 500 ms to the power conversion electronics. A photovoltaic power converter is used for optical to electrical power

  

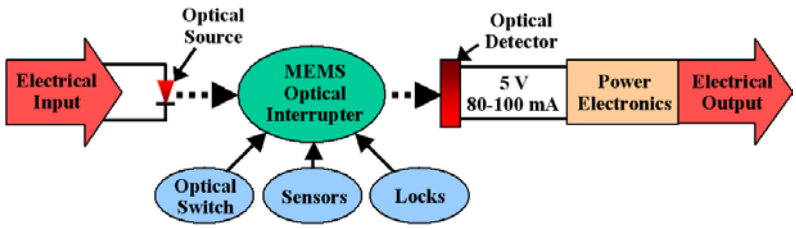


**Figure 1.** Schematic of the MEMS S&A optical charging system.

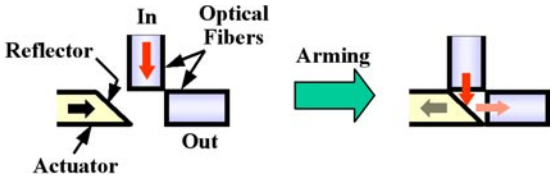


**Figure 2.** Operation of the moving reflector type optical switch.

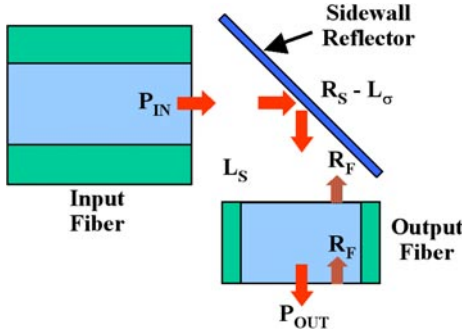


**Figure 3.** Optical losses encountered in the moving reflector optical switch.

conversion. The converter has a conversion efficiency of 0.36 $W_{out}/W_{in}$, where $W_{in}$ is the optical power input and $W_{out}$ is the electrical power output. This means that at least 1111 mW of optical power must be supplied to the detector for sufficient electrical output. It is desired to minimize the optical power required from the input LD due to electrical power requirements and heat generation considerations, so the MEMS interrupter should be as optically efficient as possible (>70%). A 70% efficient interrupter thus necessitates the use of an LD with at least a 1587 mW output.

A working wavelength of 810 nm is chosen due to the availability of commercially available, fiber pigtailed semiconductor LDs with optical output from 500 to 2000 mW. This wavelength is also within the peak conversion range for the photovoltaic converter. The LDs use large-core (50–105 $\mu$m), 0.22 numerical aperture (NA) multimode optical fibers in order to maximize coupling efficiency.

A schematic diagram of the optical switch is shown in figure 2. In this device, a bulk etched vertical sidewall reflector is actuated in and out of the optical path between input and output fibers. The fibers are placed in etched alignment grooves in the silicon wafer surface that are fabricated at 90° with respect to each other and at 45° with respect to the sidewall reflector. The reflector is located at the end of an electrostatically actuated, spring supported slider.

Fabrication is performed using Bosch process deep reactive ion etching (DRIE) [3, 4]. Several optical micro switches have been previously demonstrated using this technique [5–8]. DRIE allows the large, vertical reflector to be created that is necessary for this switch. Actuators, reflectors and fiber holding elements can all be created with a single etch step and no additional assembly is necessary other than attaching the optical fibers. Silicon on insulator (SOI) wafers are used so that released structures can be realized with an HF dip performed after the DRIE etch. The device layer thickness for the wafers used in this work is 100 $\mu$m.

## 2. System optical analysis

The optical analysis of the switch involves determining the limitations on the input and output optical fibers and predicting the optical efficiency of the system. The system efficiency is dependent upon optical losses due to less than optimum reflectivity of the etched sidewall reflector ($R_S$), scattering from the reflector surface ($L_\sigma$), Fresnel reflections at the fiber glass–air interfaces ($R_F$) and misalignments between the reflector and the input and output fibers ($L_S$). These losses are depicted in the system layout shown in figure 3. The Fresnel reflections at the input fiber glass–air interfaces are ignored because the input power ($P_{in}$) is measured before any other optical measurements are performed. The overall optical efficiency of the system can be expressed as the ratio of the measured output power ($P_{out}$) to the measured input power as shown in equation (1).

$$\frac{P_{out}}{P_{in}} = (R_S - L_\sigma)(1 - R_F)^2(1 - L_S). \quad (1)$$

### 2.1. Optical fiber losses

Large core, multimode optical fibers with an NA of 0.22 are used in order that efficient coupling is achieved between the LD and input fiber. Thus the light exiting the LD fiber will be approximately contained within a 25.4° diverging cone. The optical fibers have a standard 125 $\mu$m cladding diameter. Figures 4(*a*) and (*b*) show the optical fiber to reflector alignment. The 100 $\mu$m tall sidewall reflector limits the input fiber core to 46.3 $\mu$m in order that all the input light is confined to the reflector surface. The closest standard commercially available fiber core diameter is 50 $\mu$m. An output fiber with a 105 $\mu$m core is used in order to minimize losses due to the longitudinal fiber separation.

It should be noted that the largest optical power output that could be found from a commercially available LD with a 50 $\mu$m core fiber pigtail was 1000 mW (B&W Tek BWK-810-1.0). The 1000 mW output will not meet the minimum S&A system power requirements as outlined earlier. For the final

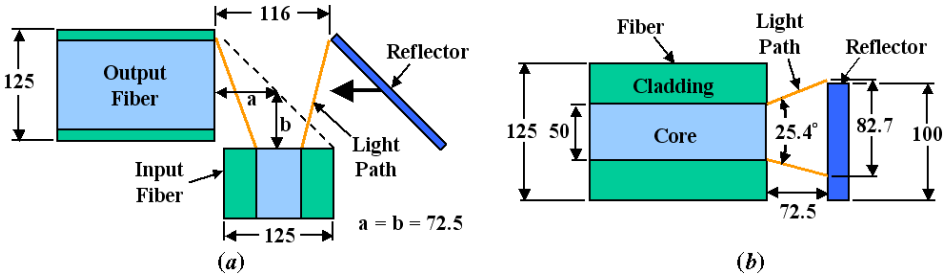


**Figure 4.** Alignment of: (*a*) optical fibers to sidewall reflector and (*b*) input fiber core to sidewall reflector.

S&A system a larger core input fiber (105 $\mu$m) will need to be used. This will necessitate the need for an SOI substrate with a thicker device layer (at least 130 $\mu$m). It was not possible to use substrates thicker than 100 $\mu$m in this study due to processing limitations.

Optical losses will be incurred in the moving reflector switch due to mechanical misalignments between the fibers and Fresnel reflections at the output fiber glass–air interfaces. The loss can be calculated with the following equation [9]:

$$R_{\mathrm{F}} = \left(\frac{n_{\mathrm{c}} - n}{n_{\mathrm{c}} + n}\right)^2. \tag{2}$$

In equation (2), $n$ and $n_{\mathrm{c}}$ are the refractive indices of air (1) and the output fiber core (1.453). Using these values, the loss at each glass–air interface due to Fresnel reflections is 3.4%. The two reflections at the output fiber interfaces will therefore reduce the maximum system optical efficiency to 93.3%. The use of AR-coated fibers will reduce the optical loss due to Fresnel reflection from 3.4% at each glass–air interfaces to less than 1%.

Mechanical misalignments between fibers include longitudinal (end face) separation, lateral (axial) displacement and angular misalignment. In this application, the fibers are held in precisely etched, 130 $\mu$m wide, 5 mm long alignment channels, so that any lateral and angular misalignments will be negligible. These misalignments are also negated by the fact that the output fiber has a much larger core than the input fiber. So any optical loss resulting from mechanical misalignment of the fibers will be due to the fiber end face separation.

The total input fiber to output fiber separation (or optical path length), $s$, measured along the central axis of each fiber, is 145 $\mu$m. The amount of light transmitted ($P_{\mathrm{out}}/P_{\mathrm{in}}$) for two fibers of equal core diameter, separated by a gap, can be calculated using a geometrical optics approach [10]. The fiber coupling efficiency, $\eta$, is found to be equal to

$$\eta = \frac{4}{\pi(NA)^2}\int_0^W \left[\arccos\left(\frac{\zeta w}{2}\right) - \left(\frac{\zeta w}{2}\right)\sqrt{1-\left(\frac{\zeta w}{2}\right)^2}\right]\frac{w}{(1+w^2)^2}\,\mathrm{d}w \tag{3}$$

with

$$W = \min\left(\frac{NA}{\sqrt{1-NA^2}}, \frac{2}{\zeta}\right). \tag{4}$$

In equations (3) and (4), $w = \tan\Theta$ and $\varsigma = s/a$ where $\Theta$ is the light divergence half angle (12.7°) and $a$ is the fiber core radius. For the case where the output fiber core is larger than the input fiber core, there will be no loss incurred until the fibers reach a certain separation, $s_0$. This separation is taken as the point at which the light from the transmitting fiber has diverged to fill an area equal to the receiving fiber core area, so that

$$s_0 = \frac{a_{\mathrm{O}} - a_{\mathrm{I}}}{\tan\Theta}. \tag{5}$$

In equation (5), $a_{\mathrm{I}}$ is the input fiber core radius and $a_{\mathrm{O}}$ is the output fiber core radius. The fiber coupling efficiency is 100% for $s \leqslant s_0$ and then equal to $\eta$ for fiber separations greater than $s_0$. In equation (3), $a$ is then taken to be equal to $a_{\mathrm{O}}$.

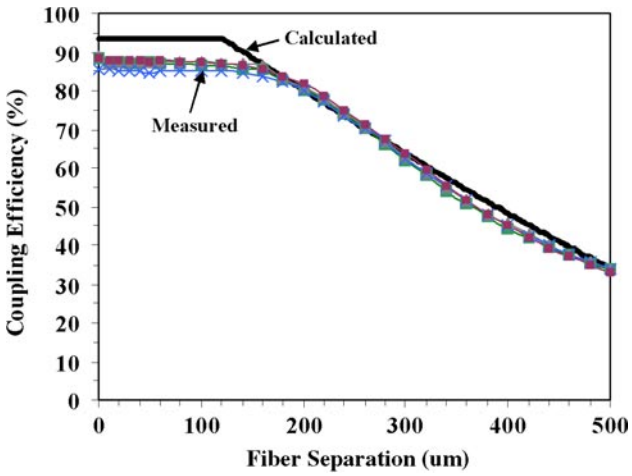


**Figure 5.** Fiber to fiber coupling efficiency versus longitudinal fiber separation (input core diameter = 50 $\mu$m, output core diameter = 105 $\mu$m). Fresnel reflection losses are included.

The calculated fiber coupling efficiency versus longitudinal fiber separation for a 50 $\mu$m core input fiber to a 105 $\mu$m core output fiber is plotted in figure 5. Also plotted are measured results (four measurements). The measurements were made by aligning an input and output fiber on a chip with a straight, etched fiber channel and etched alignment scale. The optical output power was then recorded for each fiber separation point. It should be noted that the measurements also include the Fresnel reflection losses. The calculated values have been corrected for this loss (6.7%). Discrepancies in the calculated and measured values at small separations are believed to be due to imperfections, such as scratches, on the fiber endfaces that scatter light. The total fiber related losses at a fiber separation of 145 $\mu$m are calculated to be 10.6%, while the measurements indicate an average loss of 13.9%.

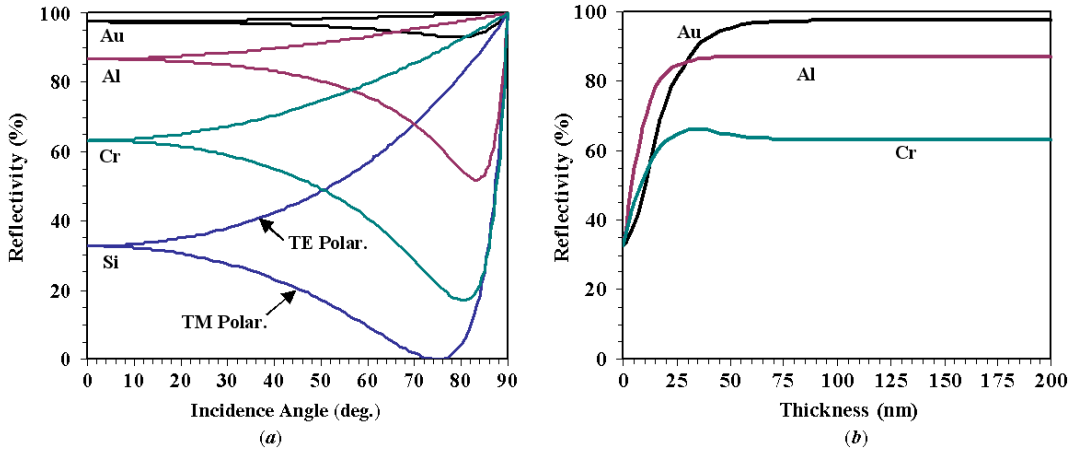


**Figure 6.** Sidewall mirror reflectivity versus (*a*) incidence angle (bulk material), and (*b*) metal film thickness (normal incidence). Working wavelength = 826.53 nm.

### 2.2. Reflector analysis

The reflectivity of an uncoated silicon surface versus angle of incidence has been calculated [11] and is plotted in figure 6(*a*). Several materials that can be used to coat the sidewall surface are also shown. The analysis assumes a bulk material and the complex index of refraction for each material was taken from tabulated values at a wavelength of 826.53 nm [12]. As can be seen, at 45° the silicon surface will only be 33% reflective for unpolarized light so that it must be coated to increase this value. The reflectivity for unpolarized light is taken as the average of the TE and TM polarization states for any given angle [11]. Au exhibits an average reflectivity of 97.5% while Al and Cr exhibit lower values of 86.2% and 62.5% respectively. Au is also the least dependent on the polarization state of the incident light.

The thin film metal on the sidewall surface must attain a certain thickness before its reflectivity will reach that of a bulk material. Reflectivity versus coating thickness for normal incidence has been calculated using standard thin film interference theory [13] and is plotted in figure 6(*b*). At a thickness of 70 nm, the Au coating attains a reflectivity of 97.1%. As expected, the Al and Cr exhibit lower reflectivities although at thinner film thicknesses. Based on these results, Au is chosen as the reflector coating material.

The calculated reflectivity values above assume a perfectly flat reflector surface so that only specular reflection will result. This will not be the case with the DRIE sidewall reflector, as the surface will attain a certain degree of roughness and scalloping from the etching process. This will result in losses from diffuse reflection (scattering), which could be significant. For a surface with a Gaussian height distribution, the ratio of scattered light to total reflected light can be estimated with the following equation [14]:

$$\frac{P_{\text{scat}}}{P_{\text{tot}}} = 1 - \exp\left[\frac{4\pi\sigma\cos\Theta}{\lambda}\right]^2 = L_\sigma. \qquad (6)$$

In equation (6), $P_{\text{scat}}$ is the amount of light scattered from the specular direction, $P_{\text{tot}}$ is the total amount of light reflected from the surface, $\sigma$ is the measured RMS surface roughness, $\Theta$ is the incident angle of the light and $\lambda$ is the wavelength of the light. The equation has been found to be accurate as long as $\sigma/\lambda \leqslant 0.3$. Figure 7 shows a plot of the total scatted light versus RMS surface roughness for a wavelength of 810 nm and incident angle of 45°. For the scattered light to stay below 10%, the RMS surface roughness must be less than 30 nm. This value is near what others have reported for measured (36 nm) DRIE sidewall surface roughness [15].

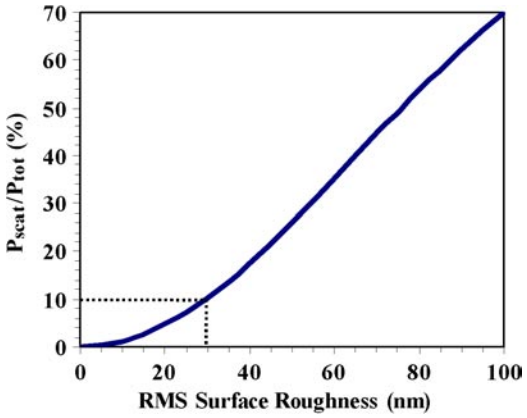


**Figure 7.** Scattered light versus reflector RMS surface roughness for $\lambda = 810$ nm and $\Theta = 45°$.

### 2.3. System optical efficiency

This section will summarize the several previous sections in order to predict the overall optical efficiency of the moving reflector type switch. A loss of 13.9% (measured) will be incurred due to the 145 $\mu$m longitudinal separation of the input and output fibers and Fresnel reflections at the output fiber glass–air interfaces. The gold-coated sidewall reflector has a theoretical maximum reflectivity of 97.5%, but scattering due to surface roughness will reduce this value. The sidewall surface roughness that will result from the DRIE process is not strictly known before fabrication, but it is believed it will range from 20 to 50 nm rms. This results in a predicted scattering loss of 4.7–26.0%. Using these values, the system optical efficiency is calculated using equation (1) and the results are shown in figure 8. At a reflector surface roughness of 20 nm rms, the system optical efficiency is predicted to be

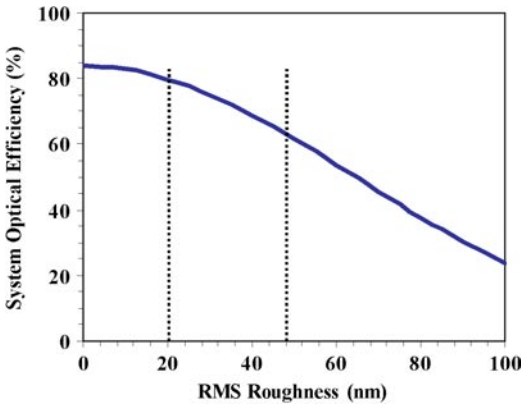


**Figure 8.** Predicted overall optical efficiency of the moving reflector type switch.

79.9% while at a roughness of 50 nm rms the efficiency falls to 61.6%.

## 3. Actuator development

### *3.1. Actuator design*

The use of large core multimode fibers necessitates the use of a large displacement actuator so that the reflector can be moved completely between the off and on positions. The minimum required displacement is 116 $\mu$m for input and output fibers positioned 72.5 $\mu$m from the sidewall reflector (see figure 4(*a*)). Although a large displacement is required, virtually no force is necessary for this application, as only light needs to be moved. These requirements point to the use of a combdrive electrostatic actuator.

The actuator used for this device has been previously demonstrated [16] and a CAD layout is shown in figure 9. The reflector design is one that is currently being used for a low-power optical circuit in the S&A system and allows for a compact switch footprint. The actuator has several key design features including variable length comb teeth and pre-bent beam springs, which increase lateral stability at large displacements [6]. One hundred comb teeth are split between two arms and suspension is provided by four, 3 mm long beam springs. The gap between the teeth is 7 $\mu$m. The actuator is capable of 200 $\mu$m displacement at a 50 V dc drive signal. This allows the reflector to be kept well away from the optical path when in the safe position.

### *3.2. Thermal considerations*

At the optical power levels present in this system, reflector failure due to thermal breakdown becomes a concern. Any light not reflected from the gold surface (theoretical maximum reflectivity is less than 100%) will be absorbed. For a long pulse or continuous wave (CW) beam incident on a metal mirror, any laser induced damage (LID) will be due to this absorption [17], which will cause the reflector and supporting structure to heat and subsequently melt.

In order to determine if excessive heating of the reflector structure will result from absorbed optical energy, an FEA thermal analysis has been performed using ANSYS software. The reflector and support structure are represented as simple, straight beams in order to ease model creation and reduce solution time. The meshed model is shown in figure 10(*a*). Heat loss is modeled as conduction through the support beams and springs to the Si base on the device layer. Heat loss due to conduction also occurs from the bottom of the support beams and springs through the 2 $\mu$m (SOI oxide layer thickness) air gap to the underlying Si handle layer [18]. The effects of convection and radiation from the beam through the air gap to the substrate are assumed negligible [19]. This is assumed true for all temperatures in order to simulate a worst-case scenario. Also, in order to simulate a worst-case scenario, a 1 $\mu$m air gap is also left between the support beam immediately behind the reflector and the Si stop. Conduction also takes place across this air gap. The bottom of the handle wafer remains at ambient temperature (300 K).

The thermal input is a heat flux applied to the face of the reflector. The value of the input heat flux (W $\mu$m$^{-2}$) is equal to the optical power density at the reflector surface for a 72.5 $\mu$m fiber face to reflector separation ($1.86 \times 10^{-4}$ W $\mu$m$^{-2}$) times the optical absorption percentage. A perfect thermal interface is assumed between the metal coating and the underlying Si

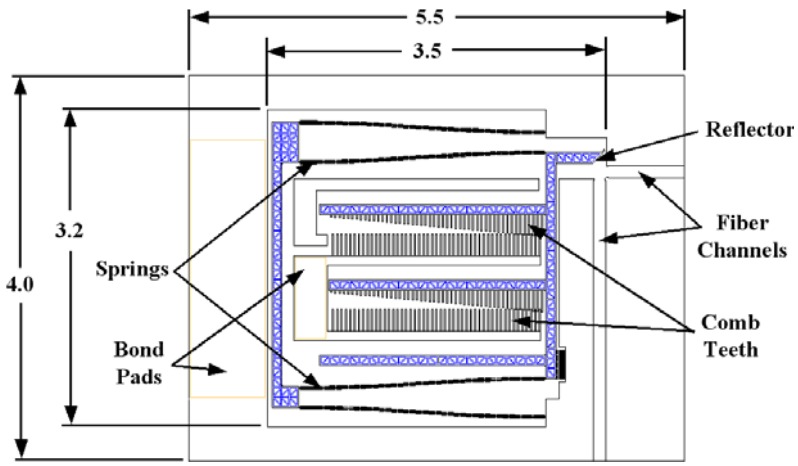


**Figure 9.** Combdrive electrostatic actuator schematic (all dimensions in mm).

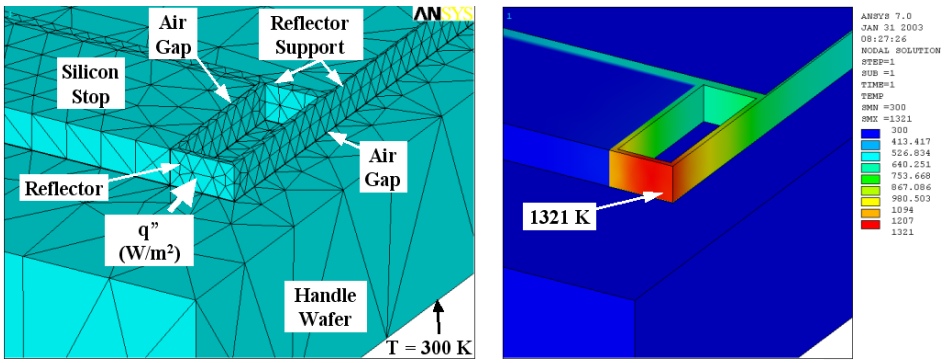


**Figure 10.** FEA thermal analysis of the sidewall reflector and support structure: (*a*) meshed FEA model and (*b*) FEA solution for an optical absorption of 26%.

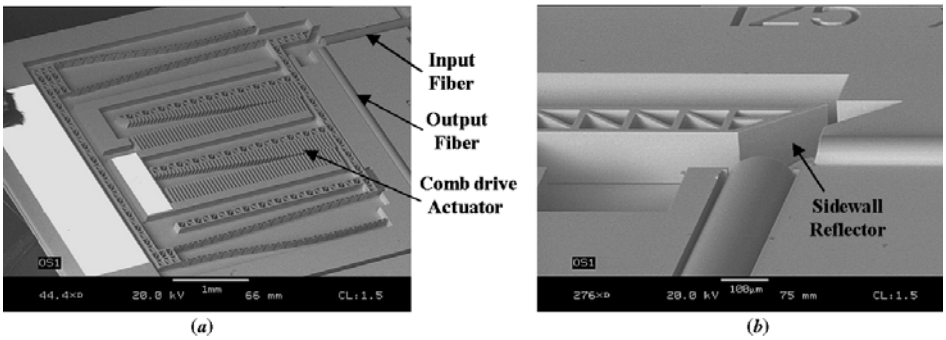


**Figure 11.** SEM micrographs of (*a*) moving reflector type optical switch and (*b*) fiber alignment to the sidewall reflector.

so that any heat generated in the coating is transferred to the support structure. The thermal conductivity of the Si remains constant at 148 W $m^{-1}$ $K^{-1}$. The reflectivity of the gold surface coating is also assumed to remain constant with temperature. A linear, 3D solid element type (SOLID70) is used so that the only degree of freedom per node is temperature. The solution is run to a steady-state temperature distribution.

The reflector surface has a maximum theoretical reflectivity of 97.5% so that the minimum absorption is 2.5%, but this value may be much higher. The actual amount of absorption is dependent upon such factors as variations in the reflector surface roughness [17] and the presence of contaminants on the reflector surface [20]. Assuming that the Au surface absorbs the minimum of 2.5% of the incident optical energy, the reflector is predicted to reach a maximum temperature of 398 K, which is well below the melting point of both Au (1336 K) and Si (1685 K) [21]. At 26% absorption, the reflector is predicted to reach a temperature of 1321 K. This solution is shown in figure 10(*b*). The most dominant thermal dissipation path is conduction through the silicon reflector support, so the size of the reflector structure could simply be increased in order to minimize heating. This, however, comes at the expense of increased device area. While these results are encouraging, they should only be taken as an indication of the degree to which the reflector will heat. This is due to the fact that the actual temperature that the reflector surface will reach is highly dependent upon the adhesion between the thin film and the underlying Si substrate [22].

## 4. Experimental results and discussion

### *4.1. Fabrication*

Device fabrication was performed in collaboration with MEMSCAP (formerly JDS Uniphase, MEMS Business Unit) in Research Triangle Park, NC. Processing consisted of a Bosch process DRIE followed by deposition of a 500 Å thick Cr adhesion layer and a 6500 Å thick Au layer for bond pads and reflector surfaces. The metal was applied by evaporation in a planetary fixture so that all sidewall surfaces would be coated. The sidewall metal is approximately 30% as thick (150 Å Cr, 2000 Å Au) as the metal on the wafer surface. The metallization is followed by a HF acid dip for buried oxide removal. This is followed by a $CO_2$ super critical drying step to prevent stiction of released devices. SEM micrographs of fabricated devices with attached optical fibers are shown in figures 11(*a*) and (*b*).

### *4.2. Optical efficiency measurements*

For most of the system optical efficiency measurements, chips with static reflectors are used instead of the complete moving reflector optical switch chips. The static test chips consist of a series of unreleased reflectors and etched fiber channels at 45° to the reflector surface and perpendicular to each other. This was primarily done in order to minimize any possible reflector heating that would occur. The overall efficiency measurements include all optical losses (misalignment, Fresnel reflections

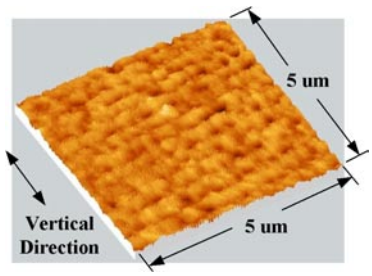


**Figure 12.** AFM scan of Au-coated, etched Si sidewall. Measured roughness is 51 nm rms.

and sidewall reflectivity). The reflectivity of the etched sidewall reflector is then calculated using equation (1).

For the input optical power, a high-power LD (B&W Tek BWK-810-1.0) with a 50 $\mu$m core fiber pigtail is used and is driven by an LD driver (Newport 5060). The power to the LD is adjusted so that the output optical power is 1000 mW for all tests. The output optical power from the 105 $\mu$m core output fiber is monitored with a thermal detector (Newport 818T-10) and power meter (Newport 1815-C).

The overall optical efficiency of the system was found to range from 44.8% to 63.7% with an average value of 53.7%. Maximum power transferred was 637 mW from the 1000 mW input. Reflectors from three wafers were tested and variability in the optical efficiency was observed from wafer to wafer. This was due to poor metallization adhesion and organic contamination on some wafers. It is believed that the organic contaminants were not completely removed during the pre-metallization cleaning process. It should also be noted that no damage was observed on any of the static reflectors tested due to the high-power optical energy.

The average system optical efficiency value is below the range predicted by the optical analysis. This is due to inaccuracies in the scattering model and a slightly rougher than expected sidewall surface, as will be described in the next section. There is also a small amount of light lost over the top of the sidewall (see figure 4(*b*)) which is not accounted for in the model. Also, it has been observed that DRIE sidewalls deviate slightly from perpendicular due to under-etching at the bottom of the wall [15], which is also not accounted for in the model. The reflectivity ($R_S$–$L_\sigma$) of the sidewall mirror can be calculated with equation (1) by using the results of the optical efficiency measurements along with the results of the fiber coupling measurements described previously. The average calculated reflectivity of the sidewall ranges from 52.0% to 73.9% with an average value of 62.8%. This is well below the maximum value for Au of 97.5% and is due to scattering from the etched sidewall.

### *4.3. Surface roughness measurements*

Surface roughness measurements of the etched sidewall reflectors were performed with an atomic force microscope (AFM). A Unitron Versamet 2 microscope was used in non-contact mode. An AFM scan is shown in figure 12 with the vertical direction of the sidewall noted. RMS roughness was found to be 51 nm rms. This is slightly higher than the expected range (20–50 nm) used for the optical efficiency calculations and higher than the previously noted value of 36 nm rms found by others.

Looking at figure 7, the 51 nm rms measured surface roughness is predicted to add an additional optical loss of approximately 27% due to scattering. Correcting the theoretical maximum reflectivity (97.5%) for this loss, the actual reflectivity for the sidewall should be 70.5%. This is higher than the average sidewall reflectivity (62.8%) that was calculated from measured data. This is most likely due to the fact that the model used for scattering loss prediction is based on a Gaussian surface height distribution. The scalloping creates a cusped surface not accounted for in the model. The rather rough surface may also somewhat shadow the evaporated metal layers further contributing to reduced reflectivity. The scalloping can be minimized by optimizing process parameters such as the frequency of alternation between the etch and passivation cycles.

The scalloping resulting from the DRIE process is evident in SEM micrographs. An example is shown in figure 13(*a*). The bottom 15–25 $\mu$m of the sidewall on some of the reflectors was also found to be degraded due to undercutting during etching. The undercutting can be seen in figure 13(*b*). However, this damage does not affect the optical performance of the reflector to a great degree because very little light is hitting this portion of the sidewall. The lateral under-etching of the sidewall can also be prevented by placing a fallout structure in front of the reflector that minimizes the gap in front of the wall [16].

### *4.4. Switching measurements*

In addition to the static reflectors, complete switches have also been tested to determine optical efficiency and dynamic performance. A silicon photodetector (Newport 818-SL) is used for the dynamic measurements due to the slow response time of the thermal detector used previously. The optical efficiency of the devices was found to range from 48.0% to 67.0% with an average value of 57.3% across three wafers. Maximum power transfer was 670 mW. The average efficiency is slightly higher than the 53.7% average measured for the static test reflectors but within the estimated error limits due to factors such as input power fluctuations. Channel isolation between the on and off switch states was measured at 32 dB.

Oscilloscope traces of the actuator driving input and photodetector output as a function of time for one of the moving reflector optical switches is shown in figure 14(*a*). The device was driven at 50 V and the optical input was again 1000 mW. Switching time from the off to on position was 10 ms while a return to the off position took approximately 3 ms. As can be seen, the stabilization of the optical signal once the maximum output is reached accounts for approximately half of the switching time from the off to on position. This is due to the settling of the reflector arm after hitting the Si stop at the fully actuated position. No stiction between the sidewalls of the reflector support and stop was observed during switching. The maximum switching frequency for the switch was found to be 60 Hz when the actuator was driven with a 50% duty cycle, square wave input. The oscilloscope trace for this frequency is shown in figure 14(*b*). For the intended S&A

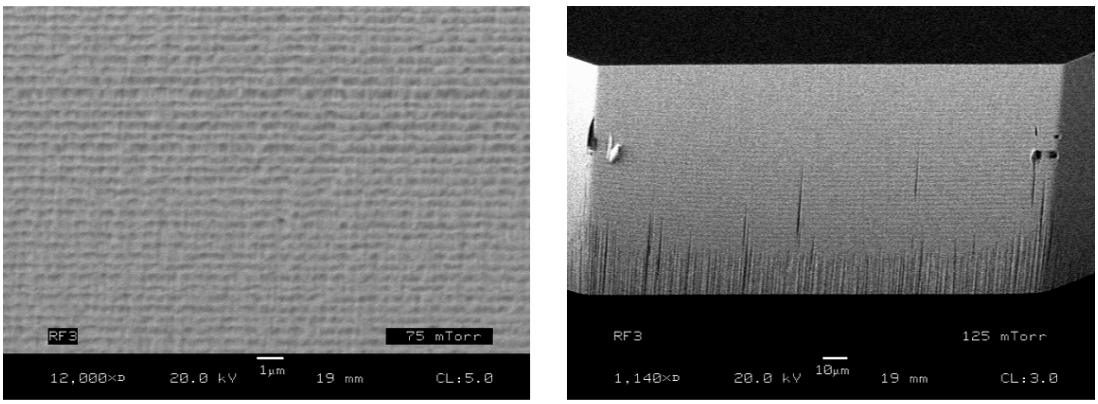


(*a*) (*b*)

**Figure 13.** SEM micrographs of DRIE sidewall reflectors: (*a*) scalloping due to the Bosch process DRIE and (*b*) undercutting on the bottom of the sidewall due to overetching.

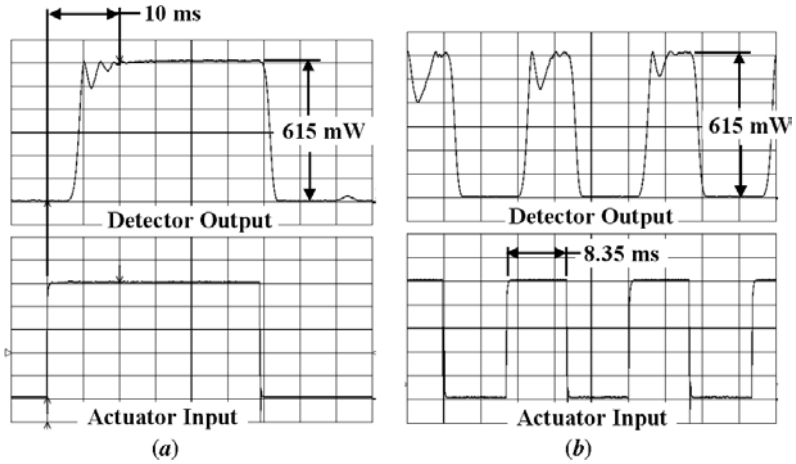


(*a*) (*b*)

**Figure 14.** Dynamic switching characteristics of the optical switch: (*a*) actuator input versus detector output and (*b*) maximum switching frequency.

application, the switch is only required to operate one time (at weapon arming) at a switching speed of 50 ms or less.

The power handling capability (LID threshold) of the released reflector design was also tested in order to verify that the high-power optical input would not result in thermal damage. Measurements were taken by increasing the optical input from an initial zero position to a maximum of 1000 mW or until failure was observed. Failure was taken as the point at which the optical efficiency took a significant drop from that observed at lower power levels.

The power handling measurements are summarized in table 1. Twelve reflectors from five different wafers were tested. Six of the twelve reflectors survived up to the maximum 1000 mW optical input in accordance with the predictions of the FEA analysis. Three of the reflectors failed after multiple (2–5) exposures to the 1000 mW input. Three of the reflectors failed at lower power levels of 800 mW or less. Looking at the data more carefully, it appears that the LID threshold is wafer dependent.

The wafer dependence of the reflector LID threshold is due to the fact that some of the wafers had poorer metallization adhesion than others, as described earlier. Although all of the wafers were fabricated with the same processing sequence,

**Table 1.** Laser induced damage threshold measurements for released reflectors.

| Wafer | Chip | Failure level (mW) | | |
|---|---|---|---|---|
| | | <800 | 1000 | >1000 |
| 1 | 1 | ■ | | |
| | 2 | ■ | | |
| | 3 | ■ | | |
| 2 | 1 | | | ■ |
| | 2 | | | ■ |
| 3 | 1 | | ■ | |
| | 2 | | ■ | |
| 4 | 1 | | | ■ |
| | 2 | | | ■ |
| | 3 | | | ■ |
| | 4 | | | ■ |
| 5 | 1 | | ■ | |

they were processed at different times. Small variations in the processing parameters could also lead to differences in the structure of the thin film metallization and its adherence to the underlying substrate. This can cause a variation in power handling capabilities of each device. Other researchers have also found that the LID threshold for thin films can vary even when processed in the same way [23].

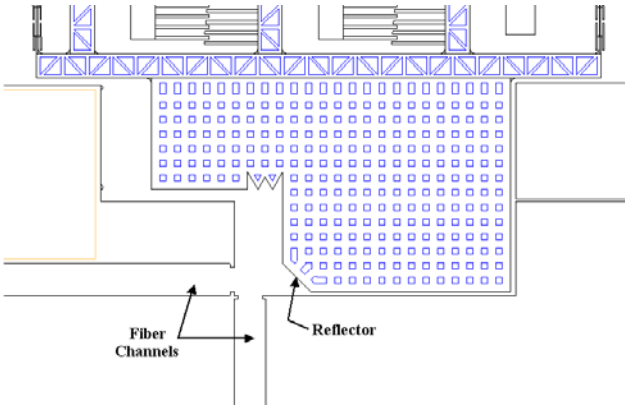


**Figure 15.** Revised reflector design to mitigate thermal failures.

Thermal failures can also be mitigated with a revised reflector design as shown in figure 15. The reflector support has been made much larger so that a more efficient thermal conduction path is created. A top chip can also be bonded to the top surface of the lower device chip so that an additional thermal conduction path is created.

## 5. Conclusion

A moving reflector type micro optical switch has been developed for high-power transfer applications. The device is a key component in a MEMS-based safety and arming system for use in underwater weapons. The switch uses a combdrive electrostatic actuator to move a Au-coated, etched sidewall reflector in and out of the optical path between two fibers. Fabrication is performed with DRIE in SOI substrates with a 100 $\mu$m thick device layer. Optical power is transferred from an 810 nm, 1000 mW LD with a 50 $\mu$m core input fiber to a 105 $\mu$m core output fiber. The average optical efficiency of the system was found to be approximately 55% for both static and released reflectors with an average sidewall reflectivity of 62.8%. Maximum power transfer for any one reflector was 670 mW from the 1000 mW input. Reflectivity is reduced significantly from an ideal surface due to the etched sidewall roughness and DRIE scalloping effects. No thermal failures of static reflectors were observed; however, several released reflectors did fail. The failures were wafer dependent and most likely due to poorly adhered metallization and contaminants. A switching time of 10 ms was achieved from the off to on state with a maximum switching frequency of 60 Hz. Channel isolation between the on and off switch states was found to be greater than 30 dB.

## Acknowledgments

The authors would like to thank DARPA and the Office of Naval Research for the funding and continued support of this research. The authors would also like to thank Dr Hugh Bruck and Huiqing Jin for the AFM imaging and Dr Brandon Choi for the SEM micrographs.

## References

[1] Fan L, Last H, Wood R, Dudley B, Malek C K and Ling Z 1998 SLIGA based underwater weapon safety and arming system *Microsyst. Technol.* **4** 168–71
[2] Beamesderfer M, Chen S, DeVoe D L, Litcher E and Johnson K 1999 Analysis of an optical energy interrupter for MEMS based safety and arming systems *Proc. SPIE: MEMS Reliability for Critical and Space Applications* vol 3880 pp 101–11
[3] Ayon A A, Chen K S, Lohner K A, Spearing S M, Sawin H H and Schmidt M A 1999 Deep reactive ion etching of silicon *Proc. Material Research Society Symp.* vol 546 pp 51–61
[4] Walker M J 2001 Comparison of Bosch and cryogenic processes for patterning high aspect ratio features in silicon *Proc. SPIE: MEMS Design, Fabrication, Characterization, and Packaging* vol 4407 pp 89–99
[5] Wang Z F, Shan X C, Wang Z P, Cao W Q, Xu J F, Lim S P, Noell W and de Rooij N 2003 Development of 1 × 4 micro optical switch based on SOI vertical micromirror technology *Proc. SPIE: MOEMS and Miniaturized Systems III* vol 4983 pp 109–13
[6] Grade J D and Jerman H 2000 A large deflection electrostatic actuator for optical switching applications *Proc. Solid-State Sensor and Actuator Workshop (Hilton Head Island, SC, 4–8 June, 2000)* pp 97–100
[7] Marxer C and de Rooij N F 1999 Micro-opto-mechanical 2 × 2 switch for single mode fibers based on plasma etched silicon mirror and electrostatic actuation *J. Lightwave Technol.* **17** 2–6
[8] Yasseen A, Mitchell J N, Klemic D, Smith D A and Mehregany M 1999 A rotary electrostatic micromotor 1 × 8 optical switch *IEEE J. Sel. Top. Quantum Electron.* **5** 26–32
[9] Keiser G 2000 *Optical Fiber Communications* (Boston: McGraw-Hill) p 209
[10] van Etten W, Lambo W and Simons P 1985 Loss in multimode fiber connections with a gap *Appl. Opt.* **24** 970–6
[11] Siegel R and Howell J R 1992 *Thermal Radiation Heat Transfer* (Washington, DC: Taylor and Francis) chapter 4
[12] Palik Edward D (ed) 1985 *Handbook of Optical Constants of Solids* (New York: Academic)
[13] Macleod H A 2001 *Thin Film Optical Filters* (Bristol: Institute of Physics Publishing) chapter 2
[14] Beckamann P A and Spizzichino A 1987 *The Scattering of Electromagnetic Waves from Rough Surfaces* (Norwood, MA: Artech House Publishers)
[15] Marxer C, Thio C, Gretillat M A, de Rooij N F, Battig R, Anthamatten B V and Vogel P 1997 Vertical mirrors fabricated by deep reactive ion etching for fiber optic switching applications *J. Microelectromech. Syst.* **6** 277–84
[16] Smith G L, Maloney J, Fan L and DeVoe D L 2001 Large displacement microactuators in deep reactive ion etched single crystal silicon *Proc. SPIE: MEMS Components and Applications for Industry, Automobiles, Aerospace, and Communication* vol 4559 pp 138–47
[17] Wood R M 1993 *Optical Materials* (London: Institute Of Materials) chapter 10
[18] Supino R N and Talghader J J 2002 Average optical power monitoring in micromirrors *IEEE J. Sel. Top. Quantum Electron.* **5** 12–8
[19] Lin L and Chiao M 1996 Electrothermal responses of lineshape microstructures *Sensors Actuators* A **55** 35–41
[20] Wood R M 1986 *Laser Damage in Optical Materials* (Bristol: Institute of Physics Publishing)
[21] Incropera F P and DeWitt D P 1990 *Fundamentals of Heat and Mass Transfer* (New York: Wiley)
[22] Metev S M and Veiko V P 1998 *Laser-Assisted Micro-Technology* (Berlin: Springer) p 41
[23] Bodefeld R, Schreiber J, Gebner H, Welsch E, Theobald W, Feurer T and Sauerbrey R 2001 Optical damage of sputtered gold films irradiated with femtosecond laser pulses *Proc. SPIE: Laser Induced Damage in Optical Materials 2000* vol 4347 pp 45–52